11th World Congress on Computational Mechanics (WCCM XI)
5th European Conference on Computational Mechanics (ECCM V)
6th European Conference on Computational Fluid Dynamics (ECFD VI)
E. Oñate, J. Oliver and A. Huerta (Eds)

QUASI BRITTLE MATRIX COMPOSITE MATERIALS: A COMPUTATIONAL APPROACH BASED ON DISCONTINUOUS-LIKE FE AND FRACTURE MECHANICS DEBONDING SIMULATION

Roberto BRIGHENTI*, Andrea CARPINTERI* and Daniela SCORZA*

* Dept. of Civil-Environmental Engng & Architecture (DICATeA)
University of Parma
Viale delle Scienze 181A, 43100 Parma, Italy
e-mail: brigh@unipr.it, www.dicatea.unipr.it

Key Words: *Fibre, Composite, Debonding, Fracture, Discontinuous FE.*

Abstract. In the present paper, the damaging mechanisms observed in fibre reinforced composite materials are simulated. In particular, quasi brittle matrix composites are examined: such cases typically involve the matrix damage associated to the creation and propagation of cracks, whose opening is mitigated by the presence of the reinforcing fibre phase. On the other hand, the effectiveness of fibres on the composite's load bearing capacity is also heavily affected by the debonding phenomenon. Both degrading mechanisms are considered in the proposed mechanical model: the matrix cracking is accounted for by adopting a discontinuous-like FE approach which allows us to consider cracks depending on the matrix stress field, whereas the fibre-matrix detachment is simulated through a crack growth model based on the critical interface fracture energy; the remote critical stress causing debonding (i.e. crack advancing) can be obtained from the interface SIF. The main mechanical aspects of the developed model are described and, through some numerical examples compared with existing literature data, the two damaging aspects are shown to properly describe the complex phenomena arising in such multiphase materials.

1 INTRODUCTION

Composites can be considered as advanced materials due to their good mechanical properties (elevated strength and modulus, high fatigue strength and fatigue damage tolerance, corrosion and wear resistance, low value of the thermal expansion coefficient, high durability, etc.) and to their tailorable characteristics regarding microstructure and mechanical properties [1, 2]. Composite materials are structural materials consisting of two or more constituents combined at a macroscopic level. Their classification is usually based on the kind of matrix material (polymers, metals, ceramics) and of reinforcing phase (fibres, particles, flakes). Among the numerous available composites, fibre-reinforced (FRC) are often used for their fabrication simplicity and affordable costs [2]: they consist of a matrix phase with a dispersion of fibres, unidirectional or randomly arranged. The matrix material transfers stresses between the fibres, is responsible for interface shear strength, and governs the damage tolerance properties of the material. Typical damage phenomena leading to a significant loss of the mechanical performance are: matrix cracking, fibre-matrix debonding, fibre breaking, fibre

instabilities [3]. In particular, matrix cracking and fibre-matrix debonding are crucial for the proper assessment of in-service safety and the optimal design of such a class of materials.

In the present paper, a micromechanical model enabling the assessment of the damage process in FRC is proposed. In particular, a discontinuous-like numerical approach is developed to simulate the matrix fracture, whereas the fibre-matrix detachment is accounted for by adopting a fracture mechanics approach, i.e. by evaluating the Stress-Intensity Factor (SIF) arising along the 3D crack corresponding to the detaches region existing between two dissimilar materials. The capability of the proposed computational approach, implemented in a FE program, is verified by assessing the cited damage phenomena occurring in short-fibre reinforced composites.

2 OVERVIEW ON DAMAGE PHENOMENA IN FIBRE-REINFORCED COMPOSITES

The main degrading effects responsible for a significant loss of composites mechanical performance are: matrix fracture, matrix crushing, fibre-matrix debonding, fibre breaking, fibre-fibre interaction, fibre instabilities [4, 5].

The reciprocal fibre interaction becomes of remarkable importance only when the fibre volume content is high (>20%), while normally the so-called dilute hypothesis can be reasonably made. Fibres interaction during fibre-matrix crack initiation and propagation represents also a crucial phenomenon, which can be taken into account through homogenization techniques applied to this class of materials [6, 7]. Failure mechanisms corresponding to fibre instabilities have also been recognised to be relevant in presence of fibre-matrix detachment [8].

Computational methods for the assessment of the above complex mechanical phenomena have been developed in the recent literature: it is worth mentioning computational techniques [9, 10] and micromechanical models [11].

3 MICROMEHANICAL MODEL

In the present section the two main degrading effects in FRC, i.e. matrix cracking and fibre debonding, are mechanically interpreted and numerically modeled.

3.1 Fracture simulation in the matrix material

Fracture in solids mathematically corresponds to a discontinuity of the displacement field along the crack line S and contained in a solid that occupies the region Ω (Fig. 1a). Such a discontinuity, the strain-displacement and stress-displacement relationships can be expressed as follows [12, 13]:

$$\boldsymbol{\delta}(\mathbf{x}) = \bar{\boldsymbol{\delta}}(\mathbf{x}) + H(\mathbf{x}) \cdot [[\boldsymbol{\delta}(\mathbf{x})]] = \bar{\boldsymbol{\delta}}(\mathbf{x}) + \underbrace{H(\mathbf{x}) \cdot \mathbf{w}(\mathbf{x})}_{\boldsymbol{\delta}_d(\mathbf{x})} \tag{1a}$$

$$\boldsymbol{\varepsilon}(\mathbf{x}) = \underbrace{\nabla^s \bar{\boldsymbol{\delta}}(\mathbf{x}) + H(\mathbf{x}) \cdot \nabla^s \mathbf{w}(\mathbf{x})}_{\boldsymbol{\varepsilon}^b(\mathbf{x})} + \underbrace{\delta_s \left(\mathbf{w}(\mathbf{x}) \otimes \mathbf{i}\right)^s}_{\boldsymbol{\varepsilon}^u(\mathbf{x})} \quad , \quad \boldsymbol{\sigma}(\mathbf{x}) = \mathbf{C} : \left[\nabla^s \bar{\boldsymbol{\delta}}(\mathbf{x}) + H(\mathbf{x}) \cdot \nabla^s \mathbf{w}(\mathbf{x})\right] \tag{1b, c}$$

where the displacement field $\boldsymbol{\delta}(\mathbf{x})$ is the sum of its continuous part, $\bar{\boldsymbol{\delta}}(\mathbf{x})$, and the discontinuous one, $\boldsymbol{\delta}_d(\mathbf{x}) = H(\mathbf{x})[[\boldsymbol{\delta}(\mathbf{x})]] = H(\mathbf{x}) \cdot \mathbf{w}(\mathbf{x})$, and $H(\mathbf{x})$ is the Heaviside jump

function placed across the crack line: i.e. $H(\mathbf{x})=0$ if $\mathbf{x}\in\Omega^-$, $H(\mathbf{x})=1$ if $\mathbf{x}\in\Omega^+$.

The displacement jump vector along the line S, $[[\boldsymbol{\delta}(\mathbf{x})]]$, represents the displacement discontinuity vector $\mathbf{w}(\mathbf{x})$ that can be expressed as the sum of the normal ($\mathbf{u}(\mathbf{x})$) and the tangential ($\mathbf{v}(\mathbf{x})$) jump displacement vectors: $\mathbf{w}(\mathbf{x})=\mathbf{u}(\mathbf{x})+\mathbf{v}(\mathbf{x})=\mathbf{i}u(\mathbf{x})+\mathbf{j}v(\mathbf{x})$ (Fig. 1b), where $\mathbf{i}$ and $\mathbf{j}$ are the unit vectors identifying the normal and tangential displacement components, respectively, ∇^s is the symmetric gradient operator, $\mathbf{Q}$ is the fourth order elastic tensor, and δ_s is the Dirac delta function located on S.

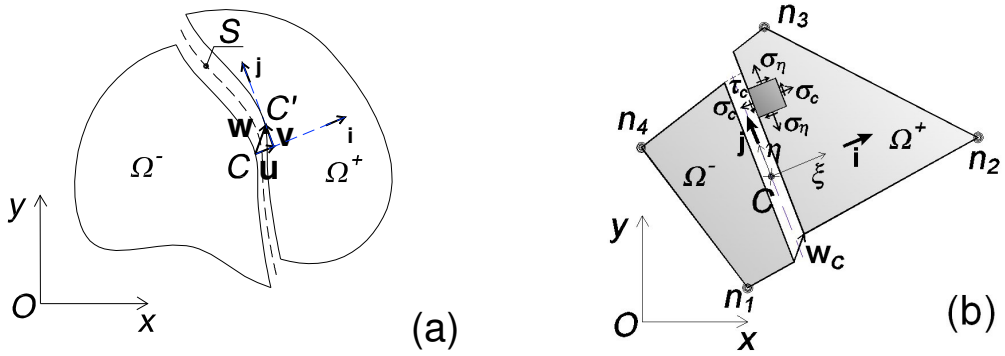

Figure 1: Discontinuous displacement field along the line S in a 2-D solid (a). Definition of the versors $\mathbf{i}$ and $\mathbf{j}$ at point C on S in a cracked finite element (b).

In Eq. (1b) the bounded, $\boldsymbol{\varepsilon}^b(\mathbf{x})$, and the unbounded, $\boldsymbol{\varepsilon}^u(\mathbf{x})$, part of the strains are indicated.

The variational formulation of the above stated problem [14] is given by:

$$\int_{\Omega\setminus S}\nabla^s(\delta\mathbf{u})\,\boldsymbol{\sigma}\,d\Omega=\int_{\Omega\setminus S}\delta\mathbf{u}\cdot\mathbf{b}\,d\Omega+\int_{\Gamma_t}\delta\mathbf{u}\cdot\hat{\mathbf{t}}\,d\Gamma+\int_{S}(\delta\mathbf{u}^+-\delta\mathbf{u}^-)\cdot\mathbf{t}^+\,d\Gamma \tag{2}$$

where $\boldsymbol{\varepsilon}$ and $\boldsymbol{\sigma}$ are the strain and stress tensors, respectively, $\mathbf{b}$ represents the body force vector, $\hat{\mathbf{s}}$ and $\hat{\mathbf{t}}$ are the prescribed displacement and tension vectors on Γ_u and on Γ_t, respectively, $\mathbf{t}^+=-\mathbf{t}^-$ is the traction transmitted across the discontinuity line S.

$\delta\mathbf{u}$ represents any kinematically admissible displacement field, where the symbol $\delta(\bullet)$ denotes a generic variation of the quantity $(\bullet)$ and $\Gamma_t^+=\Gamma_t\cap\partial\Omega^+$, $\Gamma_t^-=\Gamma_t\cap\partial\Omega^-$. The variation of the discontinuous displacements can be written as $\delta\boldsymbol{\delta}=\delta\bar{\boldsymbol{\delta}}+H\cdot\delta\mathbf{w}$, with $\delta\mathbf{w}=\delta\mathbf{u}^+-\delta\mathbf{u}^-$. By introducing the classical FE interpolation (Fig. 1b), the quantities related to the kinematically admissible displacement field $\delta\mathbf{u}$ can be written as follows:

$$\begin{aligned}
&\delta\mathbf{u}=\mathbf{N}\cdot\delta\boldsymbol{\delta}+H\cdot\delta\mathbf{w}_n-\mathbf{N}^+\cdot\delta\mathbf{w}_n=\mathbf{N}\cdot\delta\boldsymbol{\delta}+[H\cdot\mathbf{I}-\mathbf{N}^+]\cdot\delta\mathbf{w}_n\\
&\delta\boldsymbol{\varepsilon}=\nabla^s(\delta\mathbf{u})=\mathbf{B}\cdot\delta\boldsymbol{\delta}-\left[\mathbf{B}^+\otimes\delta\mathbf{w}_n\right]^s \quad \text{in} \quad \Omega\setminus S\\
&\delta\mathbf{w}=\delta\mathbf{u}^+-\delta\mathbf{u}^-=\delta[[\mathbf{u}]] \qquad\qquad \text{in} \quad S\\
&\text{and}\quad \int_{\Omega\setminus S}\nabla^s(\delta\boldsymbol{\delta})\,\boldsymbol{\sigma}\,d\Omega=\int_{\Omega\setminus S}\delta\boldsymbol{\varepsilon}\,\boldsymbol{\sigma}\,d\Omega=\int_{\Omega\setminus S}\delta\boldsymbol{\varepsilon}\,\mathbf{C}\,\boldsymbol{\varepsilon}\,d\Omega
\end{aligned} \tag{3}$$

where $\delta\boldsymbol{\delta}$ is the vector of virtual nodal displacement, $\mathbf{N}$ is the generic shape functions matrix,

$\mathbf{B}$ is the compatibility matrix of the finite element, $\mathbf{N}^+(\mathbf{x}) = \sum_{i\in\Omega_e^+} N_i(\mathbf{x})$ for $\mathbf{x}\in\Omega_e^+$, and $\mathbf{w}_n$ represents the nodal counterpart of the discontinuous displacement vector that can be interpolated as $\mathbf{w} = [H\cdot\mathbf{I} - \mathbf{N}^+]\cdot\mathbf{w}_n$ ($\mathbf{I}$ is the identity matrix). The variational statement (see Eq. (2)) becomes:

$$\begin{aligned}&\int_{\Omega\setminus S}\left[\mathbf{B}\cdot\delta\boldsymbol{\delta} - \left[\mathbf{B}^+\otimes\delta\mathbf{w}_n\right]^s\right]^t \mathbf{C}\left[\mathbf{B}\cdot\boldsymbol{\delta} - \left[\mathbf{B}^+\otimes\mathbf{w}_n\right]^s\right]d\Omega = \\ &= \int_{\Omega\setminus S}\left[\mathbf{N}\cdot\delta\boldsymbol{\delta} + [H\cdot\mathbf{I} - \mathbf{N}^+]\delta\mathbf{w}_n\right]^t \mathbf{b}\,d\Omega + \int_{\Gamma_t}\left[\mathbf{N}\cdot\delta\boldsymbol{\delta} + [H\cdot\mathbf{I} - \mathbf{N}^+]\delta\mathbf{w}_n\right]^t \hat{\mathbf{t}}\,d\Gamma + \int_S \delta\mathbf{w}^t\,\mathbf{t}^+ d\Gamma\end{aligned} \tag{4}$$

or, in incremental form, once the variations are independently assumed to be equal to zero ($\delta\mathbf{w}_n = \mathbf{0}$ and $\delta\boldsymbol{\delta} = \mathbf{0}$) and a static condensation is done:

$$\begin{cases} d\mathbf{w} = \mathbf{K}_{ww,S}^{-1}\left(-\mathbf{K}_{w\delta}\,d\boldsymbol{\delta}\right) \\ d\boldsymbol{\delta} = \left(\mathbf{K}_{\delta\delta} - \mathbf{K}_{\delta w}\mathbf{K}_{ww,S}^{-1}\mathbf{K}_{w\delta}\right)^{-1} d\mathbf{f}_1 = \overline{\mathbf{K}_{\delta\delta}}^{-1} d\mathbf{f}_1 \end{cases} \tag{5}$$

where $\mathbf{K}_{ww,S} = \mathbf{K}_{ww} + \mathbf{K}_S$, $\mathbf{K}_S = \int_S \left[H\cdot\mathbf{I} - \mathbf{N}^+\right]^t \mathbf{T}\cdot\left[H\cdot\mathbf{I} - \mathbf{N}^+\right] d\Gamma$ ($\mathbf{T}$ is a proper operator which relates the crack tractions $d\mathbf{t}$ to the crack jump displacements, $d\mathbf{t} = \mathbf{T}\cdot d\mathbf{w}$, traction-jump law in incremental form), and $\overline{\mathbf{K}_{\delta\delta}} = (\mathbf{K}_{\delta\delta} - \mathbf{K}_{\delta w}\mathbf{K}_{ww,S}^{-1}\mathbf{K}_{w\delta})$ is the condensed tangent stiffness matrix of the cracked finite element.

A finite element (Fig. 1b) where a discontinuity of the displacement field takes place along a straight line S (centered in its geometrical centre C, crossing the element in an arbitrary direction given by the unit vector $\mathbf{j}$) is herein examined. The FE displacement field $\mathbf{s}(\mathbf{x})$ can be written (see Eq. (1)) as $\mathbf{s}(\mathbf{x}) = \mathbf{N}(\mathbf{x})\cdot\boldsymbol{\delta} + \left[H(\mathbf{x})\mathbf{I} - \mathbf{N}^+(\mathbf{x})\right]\cdot\mathbf{w}_n$, whereas the displacement jump vector in the centre of the element is expressed as $\mathbf{w}_C = \mathbf{u}_C + \mathbf{v}_C$, $\mathbf{u}_C$ and $\mathbf{v}_C$ being the displacements jumps normal and parallel to the crack line, respectively.

A strategy [12, 13] is used to simulate the localisation phenomenon corresponding to fracture: the mechanical effect of a crack in a material produces a sudden reduction of the stress normal to the crack line and, eventually, allows a shear stress between the crack faces to exist. By properly modifying the element stress field due to the crack effect, such a phenomenon can be simulated in a way similar to that of the non-linear material behaviour occurring in the classical elastic-plastic FE formulation. The above description of the crack presents the advantage to keep the continuity of the displacement field inside each finite element, since it acts only at the stress level, without the need of special or enriched shape functions to represent the discontinuous displacement field.

The obtained non-linear problem can be iteratively solved by driving the unbalanced nodal force vector $\mathbf{f}_{e,u}^{(i)}$ to very small values, according to a proper vector norm. For a given load step *i*, the unbalanced nodal force vector $\mathbf{f}_{e,u}^{(i)}$ in a generic finite element *e* can be evaluated through the following expression:

$$\mathbf{f}_{e,u}^{(i)} = \mathbf{f}_{e,ext}^{(i)} - \int_{\Omega_e} \mathbf{B}^t\cdot\boldsymbol{\sigma}_{rel}(\mathbf{w}_c)\,d\Omega \tag{6}$$

where $\mathbf{f}_{e,ext}^{(i)}$ is the external nodal force vector, whereas $\boldsymbol{\sigma}_{rel}(\mathbf{w}_c)$ is the stress tensor evaluated in the finite element fulfilling the proper stress reduction requirements.

The fracture occurrence is assumed to start when the maximum principal stress $\sigma_1(C)$ reaches the material tensile strength f_t, leading to a crack placed at the finite element midpoint C along a straight line S, oriented normal to the current maximum principal stress direction $\mathbf{i}$ (Fig. 1b). The stress field in the material surrounding the crack is thus modified obeying the normal $\sigma_c(u_c)$ and shear $\tau_c(u_c, v_c)$ bridging stresses determined on the basis of the relative crack faces displacement vector $\mathbf{w}_c = \mathbf{u}_c + \mathbf{v}_c = u_c\,\mathbf{i} + v_c\,\mathbf{j}$. Such stresses are evaluated through a cohesive-friction law [14] by using the following expressions [15]:

$$\sigma_c(u_c) = f_t \cdot e^{\frac{2 f_t (u_0 - u_c)}{2G_f - f_t \cdot u_0}} \tag{7a}$$

$$\tau_c(u_c, v_c) = \begin{cases} \operatorname{sign}(v_c) \cdot [\sigma_c(u_c) \cdot \beta] \cdot \left[1 - \left(\dfrac{u_c}{2 \cdot r_c} \right)^m \right] & \text{if } 0 < u_c < 2 \cdot r_c \quad \text{and } v_c \neq 0 \\ 0 & \text{if } u_c > 2 \cdot r_c \quad \text{or} \quad v_c = 0 \end{cases} \tag{7b}$$

where f_t is the maximum tensile strength of the material, u_0 is the lower crack opening limit at which the bridging process starts, and G_f is the fracture energy of the material. Eq.(7a) is suitable for computational reasons being continuous, derivable and never equal to zero, i.e. $\sigma_c(u_c) \underset{u_c \to \infty}{\to} 0^+$, whereas Eq.(7b) has the following mechanical interpretation: when the crack surface asperities are in contact (i.e. when $0 < u_c < 2 \cdot r_c$), a certain amount of shear stress exists between the crack faces and is expressed by a decreasing law of the relative crack distance u_c, which is a Coulomb-like friction law characterized by the friction coefficient β. The shear stress is equal to zero, $\tau_c(u_c) = 0$, when the contact between the two surfaces disappears (i.e. if $u_c > 2 \cdot r_c$) or when the sliding displacement v_c is equal to zero. If the crack is completely closed ($u_c = 0$), the crack is able to transmit a shear force obeying the Coulomb law, $\tau_c(u_c, v_c) = \operatorname{sign}(v_c) \cdot \sigma_c(u_c) \cdot \beta$, if $v_c \neq 0$. The exponent m in Eq. (7b) allows us to control the decrease of the friction coefficient, as can be reasonable to occur by increasing the relative crack distance.

The released stress state in the cracked element is written as follows:

$$\boldsymbol{\sigma}_{rel}(\mathbf{w}_c) = \mathbf{R}^t\, \boldsymbol{\sigma}_{rel,S}(\mathbf{w}_c)\, \mathbf{R} = \boldsymbol{\sigma} - \boldsymbol{\sigma}_{jump}(\mathbf{w}_c), \tag{8}$$

$$\text{with} \quad \boldsymbol{\sigma}_{rel,S}(\mathbf{w}_c) = \begin{bmatrix} \sigma_c(u_c) & \tau_c(u_c) \\ \tau_c(u_c) & \sigma_\eta \end{bmatrix}$$

where $\mathbf{R}$ is the rotation matrix between the $x-y$ and the $\xi-\eta$ co-ordinate systems (Fig. 1b). Since the discontinuity vector $\mathbf{w}_c$, evaluated in the centre of the finite element, is assumed to be constant across the element, it can give raise to an apparently discontinuous crack opening displacement across the elements boundaries. Since the crack is herein

modeled not as an effective displacement discontinuity but only through its static effect, the stress reduction in the cracked FE also produces an increase of the nodal displacement of the adjacent elements, assuring a globally continuous displacement field.

3.2 Fibre-matrix homogenization

The overall mechanical behaviour of a short-fibre reinforced composite can be analysed by writing an energy balance between the effective and the averaged strain energy density in such a heterogeneous material. The tangent elastic tensor $\mathbf{C}'_{eq}$ of the homogenized material can be written as follows [16]:

$$\mathbf{C}'_{eq} = \mu \cdot \mathbf{C}'_{m} + \eta \cdot E'_{f} \cdot \left[s(\varepsilon_f^m) + \varepsilon_f^m \cdot \frac{ds(\varepsilon_f^m)}{d\varepsilon_f^m} \right] \cdot \int_{\Phi} p_\varphi(\varphi) \cdot p_\theta(\theta) \cdot \mathbf{F} \otimes \mathbf{F} d\Phi \tag{9}$$

where μ, η are the fibre and matrix volume fractions, $\mathbf{C}'_{m}, E'_{f}$ the tangent tensor and the elastic modulus of the matrix material and the fibres, respectively, whereas $p_\varphi(\varphi), p_\theta(\theta)$ are the probability distribution functions describing the fibres arrangement in the space and $\mathbf{F} = \mathbf{k} \otimes \mathbf{k}$ is a second-order tensor. The sliding function $s(\varepsilon_f^m) = \varepsilon_f / \varepsilon_f^m$ can be evaluated once the debonded fibre length is determined (see next section).

3.3 Fibre-matrix interaction and debonding

Fibre-matrix mechanical interaction and detachment can be considered as a fracture phenomenon occurring in an elastic bi-material coupling [17,18]. The extension of such a problem to the 3D case can be used to describe the fracture phenomenon represented by a cylindrical crack arising in a partially debonded cylindrical fibre (Fig. 2), that is, the detached zone (fibre-matrix debonding) can be assumed to be a 3D cylindrical crack lying between two different materials [19,20].

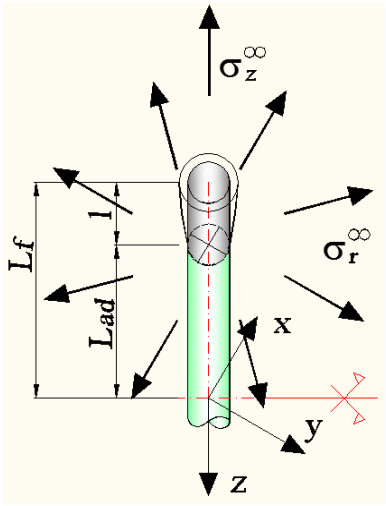

Figure 2: Debonded extremity of a fibre under remote radial (σ_x^∞) and axial (σ_z^∞) stress.

By considering the generic case of an elastic fiber embedded in an elastic matrix under remote axial (σ_z^∞) and radial (σ_r^∞) stresses (Fig 2), a mixed mode of fracture arises and the energetically equivalent SIF can be defined as follows [21]:

$$K_i = \begin{cases} \sqrt{K_I{}^2(\sigma_r^\infty) + \left[K_{II}(\sigma_r^\infty) + K_{II}(\sigma_z^\infty)\right]^2} & \sigma_r^\infty > 0 \\ K_{II}(\sigma_z^\infty) & \sigma_r^\infty \le 0 \end{cases} \tag{10}$$

Note that, in first approximation, the remote axial stress produces only a Mode II SIF, while the remote radial stress is mainly responsible for Mode I and Mode II SIFs. The above SIFs, $K_I(\sigma_r^\infty), K_{II}(\sigma_r^\infty)$, $K_{II}(\sigma_z^\infty)$, can be conveniently rewritten in a dimensionless form as $K^*_{Mw} = K_M(\sigma_w^\infty)/(\sigma_w^\infty\sqrt{\pi l})$ where $K_{Mw} = K_M(\sigma_w^\infty)$ indicates the generic Mode M SIF ($M = I, II$) due to the remote stress σ_w^∞ ($w = r, z$), and K^*_{Mw} is the corresponding dimensionless value. The equivalent SIF K_i at the fiber-matrix interface crack front (see Eq. (10)) can be also used to define the condition of unstable crack propagation (i.e. $K_i = K_{ic} = \sqrt{E_i \cdot \mathcal{G}_{ic}}$ plane stress; $= \sqrt{E_i \cdot \mathcal{G}_{ic}/(1-\nu_i^2)}$ plane strain), where $\mathcal{G}_{ic}$ is the interface fracture energy, K_{ic} is the corresponding fracture toughness, E_i and ν_i are the Young modulus and the Poisson ratio of the interface, respectively [14]. Such a fracture mechanics approach allows us to use the classical crack growth rate equations for the assessment of the stable crack propagation produced by repeated loading.

In Fig. 3, the dimensionless SIF is plotted against the relative fibre debonded length ξ for different values of Young modulus and fibre aspect ratio η: the Mode I and Mode II SIFs, due to remote radial and axial stresses, respectively, decrease with the fibre detachment. Results by Wüthrich [22] are also shown. In Fig. 4, the axial-radial remote stress ratio enabling continuous fibre detachment is plotted against the relative fibre debonded length for different values of the radial stress. According to Fig. 4, the remote axial stress allowing fibre detachment is an increasing function of ξ.

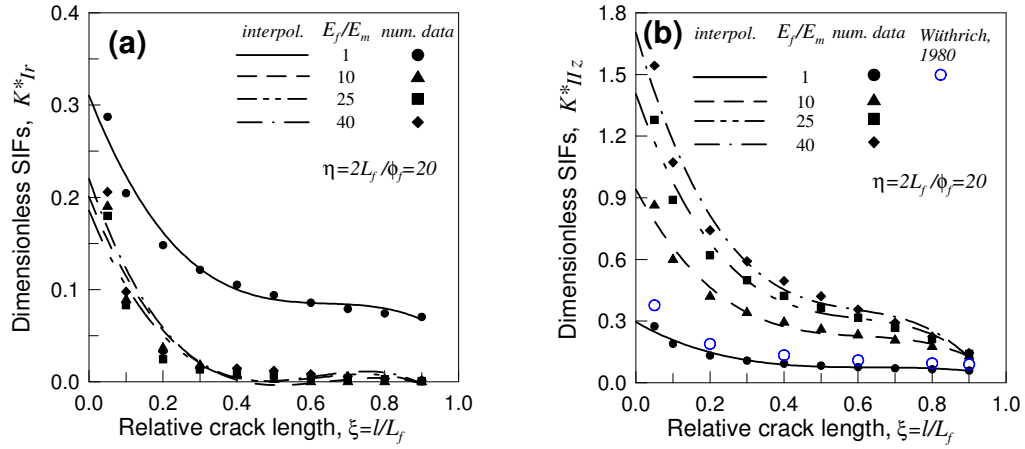

Figure 3: Dimensionless Mode I (a) and Mode II (b) SIFs due to a remote uniform radial and axial stress, respectively, against the relative crack length, for fibre aspect ratio η =20 and different values of Young modulus ratio $\gamma = E_f / E_m$.

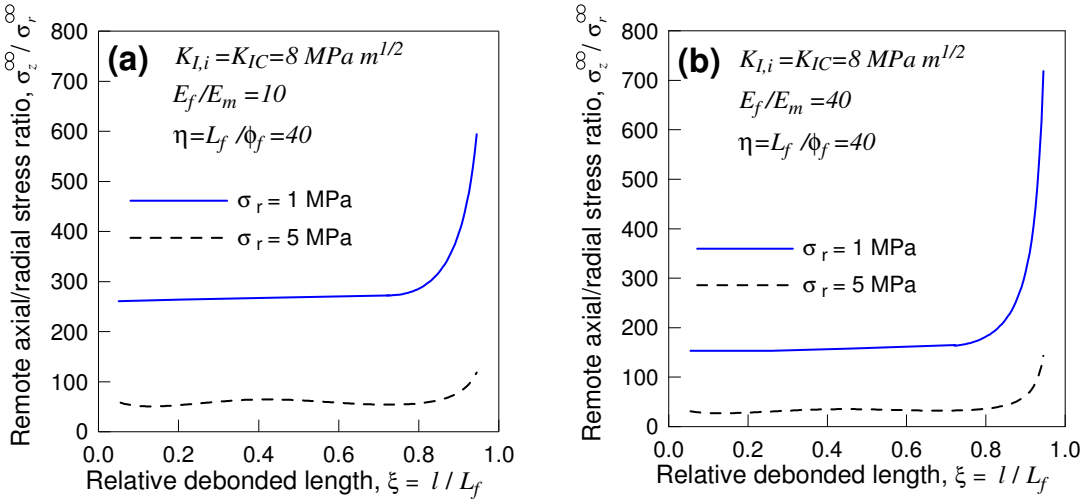

Figure 4: Dimensionless remote axial stress $\sigma_z^\infty / \sigma_r^\infty$ against the relative debonded length $\xi = l / L_f$: (a) $E_f / E_m = 10$, (b) $E_f / E_m = 40$.

5 NUMERICAL APPLICATIONS

In the present section, the problem of the failure behaviour of FRC prismatic single-edge notched concrete specimens under three-point bending is examined [23]. The specimens have span of 500mm and cross section of 150x150mm; the notch depth is equal to 25mm and its width is equal to 4mm (see beam geometry and adopted discretization in Fig. 5b). Plain and steel fibre-reinforced concretes (with random fibre distribution and two different fiber orientations, $\varphi = 0°$ and $45°$) are analysed. The mechanical parameters of the beam material are the following: Young modulus $E = 32\,\text{GPa}$, ultimate tensile strength $f_t = 2.6\,\text{MPa}$, fracture energy $G_f = 94\,\text{N/m}$. The relevant parameters for the steel fibres reinforced beams are: $\eta_f = 0.45\%$, $E_f = 210\,\text{GPa}$, $2L_f = 50\text{mm}$, $\phi_f = 1\text{mm}$, $\tau_{au} = 1\,\text{MPa}$. The analysis is performed under displacement control, by imposing a progressive vertical displacement at the top central loaded point. A plane stress condition is assumed.

Vertical load against crack mouth opening displacement (CMOD) for plain concrete and for steel fibre-reinforced concrete specimens are shown in Figs 5a and 5b, respectively. Literature numerical and experimental results are also reported [23]. As can be noted, the presence of the reinforcing fibres produces a slight increment of the peak load, but the most evident effect is an increse of ductility in the decreasing branch of the force-CMOD curve. This behaviour is significant for fibres oriented normally to the crack direction ($\varphi = 0°$), while it is less pronounced for random fibres and for $\varphi = 45°$. The agreement of the present results with the experimental and numerical ones appears to be satisfactory.

The second example considers the mixed-mode fracture behaviour of a four-point shear loaded single-edge notched beam [15]. A plane stress condition is assumed. The mechanical parameters of the beam material are the following: Young modulus $E = 35GPa$, ultimate tensile strength $f_t = 28MPa$, fracture energy $G_f = 100\,\text{N/m}$. Both plain and fibre reinforced

cases are examined. The mechanical parameters of the steel fibres are $E_f = 200GPa$, $2L_f = 24\,\text{mm}$, $\phi_f = 0.5\,\text{mm}$, $\tau_{au} = 5\,MPa$, $\tau_{fu} = 0.1 \cdot \tau_{au}$, their valume fraction is equal to $\eta_f = 5\%$ and two fiber orientations are analysed, randomly and $\varphi = 0°$. A 776 four-node bilinear FE regular mesh is adopted. The analysis is performed under displacement control [24].

The sliding function s and the dimensionless crack length $\xi = l / L_f$ distributions are plotted in Fig. 6 for load levels equal to 50% and 100% of the maximum applied load. It can

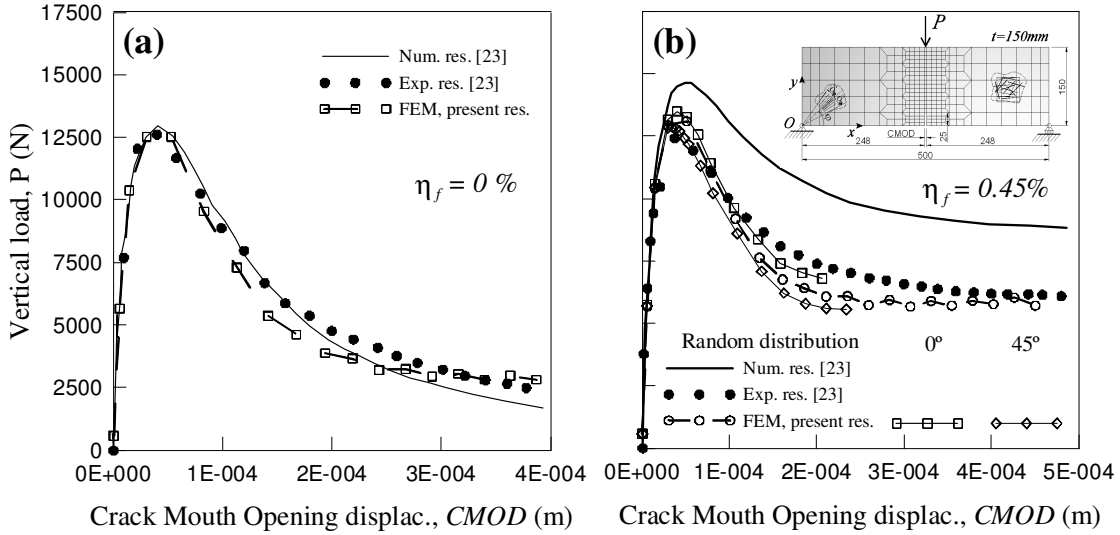

Figure 5: Vertical load vs crack mouth opening displacement (CMOD) for a three-point bending concrete beam [23]: (a) without steel fibers; (b) with steel fibers.

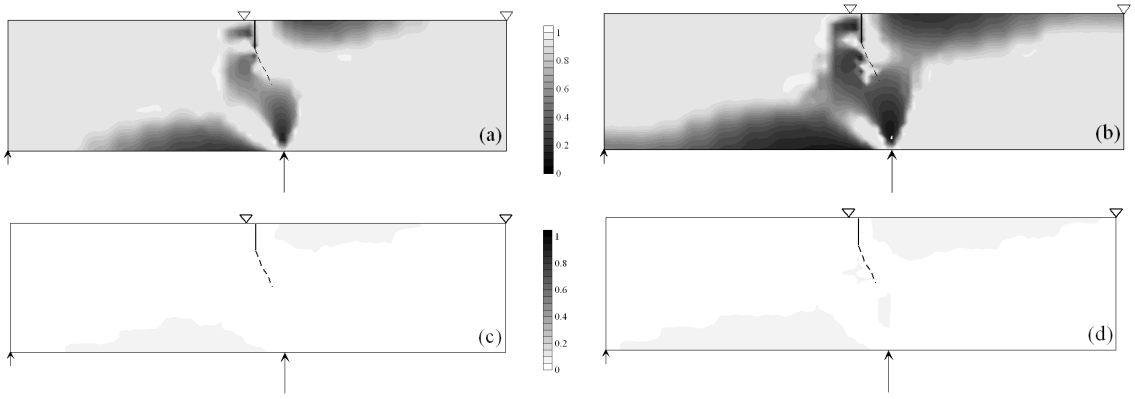

Figure 6: Dimensionless sliding function (s) in the notched beam for the case of horizontal fibres ($\varphi = 0°$) for load level equal to (a) 50% and (b) 100% of its final value; (c, d) dimensionless debonded length (ξ) for the same fibre orientation and load levels as for cases (a, b).

be noted that fibre effectiveness, represented by s, decreases with the load increment in the tensile zones of the beam and, correspondingly, the fibre debonding appears nearly in the same regions. The overall behaviour of the beam is correctly represented by the proposed model.

6 CONCLUSIONS

In the present paper, the two main degrading mechanisms (matrix cracking and fibre debonding) occurring in FRC composites are examined and numerically modeled through a micromechanics approach. Matrix fracture is accounted for by adopting a discontinuous-like FE approach, which allows us to consider cracks depending on the matrix stress field, whereas the fibre-matrix detachment is simulated through a fracture mechanics approach based on the critical interface fracture energy for crack growth. The main mechanical aspects of the developed model are discussed and, through some numerical examples, compared with some literature data. The two damaging aspects are shown to properly describe the complex phenomena arising in such multiphase materials.

REFERENCES

[1] Jones, R.M.A. *Mechanics of Composite Materials*, (Second Edition), Taylor & Francis Group (1999).

[2] Cheng, Q.G. *Fiber Reinforced Composites*. Nova Science Publishers, Inc., Hauppauge, NY, 2012.

[3] Hill, R. Theory of mechanical properties of fibre-strengthened materials: I. Elastic behaviour. *J. Mech. Phys. Sol.* (1964) 12: 199–212.

[4] Zhanga, J. and Li, V.C. Simulation of crack propagation in fiber-reinforced concrete by fracture mechanics. *Cement and Concrete Research* (2004) **34**: 333–339.

[5] Ju J.W. and KO, Y.F. Effective elastoplastic damage mechanics for fiber reinforced composites with evolutionary partial fiber debonding. *Int. J. Damage Mech.* (2008) **17**: 493–537.

[6] Greco, F. and Luciano, R. A theoretical and numerical stability analysis for composite microstructures by using homogenization theory, *Compos. Part B* (2011) **42**(3): 382–401.

[7] Greco, F. Leonetti, L. and Lonetti, P. A two-scale failure analysis of composite materials in presence of fiber/matrix crack initiation and propagation. *Compos. Struct.* (2013) **95**: 582–597.

[8] Kyriakides, S., Arseculeratne, R., Perry, E.J. and Liechti E.J. On the compressive failure of fiber-reinforced composites. *J. Sol. Struct*. (1995) **32**: 689–738.

[9] Fish, J. Yu, Q. and Shek, K. Computational damage mechanics for composite materials based on mathematical homogenization. *Int. J. Num. Meth. Engng* (1999) **45**: 1657−1679.

[10] Radtke, F.K.F., Simone, A. and Sluys L.J. A partition of unity finite element method for simulating non-linear debonding and matrix failure in thin fibre composites. *Int. J. Numer. Meth. Engng* (2011) **86**: 453–476.

[11] Brighenti, R. Carpinteri, A. and Scorza, D. A computational approach to evaluate the mechanical influence of fibres on brittle-matrix composite materials. *Comput. Mat. Sci*. (2012) **64**: 212–215.

[12] Carpinteri, A. and Brighenti, R. A new continuum FE approach for fracture mechanics discontinuous problems, *Comput. Mat. Sci*. (2009) **45**: 367–377.
[13] Brighenti, R. and Scorza, D. Numerical modelling of the fracture behaviour of brittle materials reinforced with unidirectional or randomly distributed fibres. *Mech. Mat.* (2012) **52:** 12–27.
[14] Hillerborg, A., Modéer, M. and Peterson, P.E. Analysis of crack formation and crack growth in concrete by means of fracture mechanics and finite elements, *Cement Concrete Res.* (1976) **6**: 773–782.
[15] Alfaiate, J., Wells, G.N. and Sluys, L.J. On the use of embedded discontinuity elements with crack path continuity for mode-I and mixed-mode fracture. *Engng. Fract. Mech.* (2002) **69**: 661–686.
[16] Brighenti, R. and Scorza, D. A micro-mechanical model for statistically unidirectional and randomly distributed fibre-reinforced solids, *Math. Mech. Sol.* (2012) **17**: 876–893.
[17] Rice, J.C. Elastic fracture mechanics concepts for interfacial cracks. *J. Appl. Mech.* (1988) **55**: 98–103.
[18] Hutchinson, J.W., Mear, M.E. and Rice, J.C. Crack paralleling an interface between dissimilar materials. *J. Appl. Mech.* (1987) **54**: 828–832.
[19] Zbib, H.M., Hirth, J.P. and Demir, I. The stress intensity factor of cylindrical cracks. *Int J. Engng Sci.* (1995) **33**: 247–253.
[20] Chaudhuri, R.A. Three-dimensional singular stress field near a partially debonded cylindrical rigid fibre. *Comp. Struct.* (2006) **72**: 141–150.
[21] Brighenti, R., Carpinteri, A. and Scorza, D. Fracture mechanics approach for a partially debonded cylindrical fibre. *Comp. Part B: Engng* (2013) **53**: 169–178.
[22] Wüthrich, C. Stress intensity factors for cylindrical cracks in long cylinders. *Engng Fract. Mech* (1980) **13**: 987–990.
[23] Buratti, N., Mazzotti, C. and Savoia M. Post-cracking behaviour of steel and macro-synthetic fibre-reinforced concretes, *Constr Build Mater* (2011) **25**: 2713–2722.
[24] Brighenti, R., Carpinteri, A., Spagnoli, A. and Scorza, D. Continuous and lattice models to describe crack paths in brittle–matrix composites with random and unidirectional fibres, *Engng Fract. Mech* (2013) **108**: 170–182.